Available online at www.sciencedirect.com

SciVerse ScienceDirect

journal homepage: www.elsevier.com/locate/he

Design and implementation of interleaved boost converter for fuel cell systems

*R. Seyezhai**, *B.L. Mathur*

Department of EEE, SSN College of Engineering, Chennai, India

ARTICLE INFO

Article history:
Received 23 August 2011
Received in revised form
15 September 2011
Accepted 16 September 2011
Available online 22 October 2011

Keywords:
Fuel cell
Directly coupled IBC
SiC
Switching losses

ABSTRACT

Fuel cell is one of the promising renewable and sustainable power sources because of its high power density and very low emission. It can be utilized as a clean power source for various applications such as portable electronic appliances, transportation and residential building. In order to design a highly efficient fuel cell power system, a suitable DC–DC converter is required. Among the various topologies of DC–DC converters, interleaved boost converter (IBC) has been proposed as a suitable interface for fuel cells to convert low voltage high current input into a high voltage low current output. The advantages of interleaved boost converter compared to the classical boost converter are low input current ripple, high efficiency, faster transient response, reduced electromagnetic emission and improved reliability. In the proposed interleaved converter, the front end inductors are magnetically coupled to improve the electrical performance and reduce the weight and size. This paper focuses on a three-phase directly coupled IBC using CoolMOS transistor and Silicon carbide (SiC) diode instead of the classical two-phase reported in the literature based on the tradeoff between the ripple content, cost and complexity. Mathematical analysis of overall current ripple, design equations and switching loss studies for IBC have been presented. Simulation of IBC interfaced with fuel cells have been performed using MATLAB/SIMULINK. Hardware prototypes have been built to validate the results.

1. Introduction

Fuel cells have gained attention in recent years as an attractive technology for growing energy request and cleaner environment [1,2]. Among several types of fuel cells, Proton Exchange Membrane Fuel Cell (PEMFC) is chosen for this work because of its features like low operating temperature, fast start-up, low sensitivity to orientation, long cell and stack life and low corrosion [3]. Fuel cells operate at low DC voltages (typically 600 mV per cell) and therefore a number of cells are connected in series. As a long string of cells is difficult to operate, DC–DC boost converter is generally used to further boost the voltage to the required level. Various topologies such as boost, buck and series resonant full-bridge and push-pull converters have been proposed in the literature [4,5]. But these topologies add objectionable ripples in the current flowing out of the fuel cell. To minimize the ripples, an IBC has been proposed as an interface for fuel cells as it reduces the source current ripple. In addition, interleaving provides high power capability, modularity and improved reliability [6]. A three-phase directly coupled IBC using CoolMOS switches has been proposed in this paper compared to the conventional 2-phase IBC. The application of coupled inductor in IBC where a core is shared by multiple converters results in reduced parts count, volume and weight, improved input and inductor current ripple characteristics.

* *Corresponding author*. Fax: +91 44 27474844/45/46x230.
E-mail addresses: seyezhair@ssn.edu.in (R. Seyezhai), blmathur@ssn.edu.in (B.L. Mathur).
0360-3199/$ – see front matter
doi:10.1016/j.ijhydene.2011.09.082

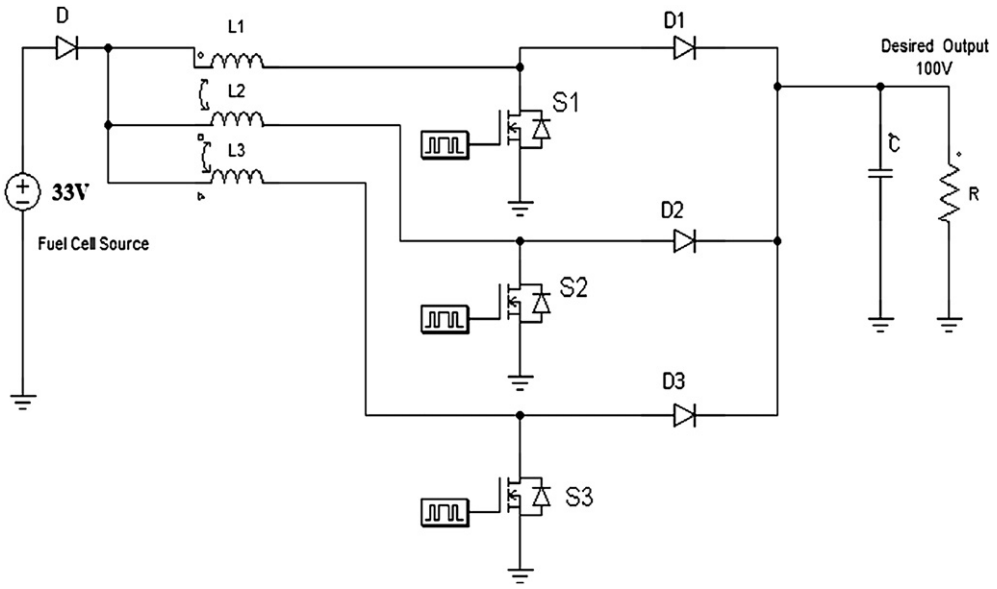

Fig. 1 – Schematic Diagram of a 3-phase directly coupled IBC.

The performance of IBC has been investigated over the operating range of the PEM fuel cell. The relationship between phase current ripple, input current ripple versus duty ratio and coupling coefficient has been analyzed. The expression for equivalent inductance has been derived. The switching losses of two sets of device combinations for IBC have been compared: the MOSFET IRFP460A and the Si diode MUR1560, the CoolMOS transistor and SiC Schottky diode CSD 100060. The performance of 3-phase directly coupled IBC has been compared with uncoupled IBC. Gating pulses are generated using PIC microcontroller. The proposed directly coupled IBC for fuel cell applications has excellent current sharing performance and reduced current ripple. Computer simulations have been done and hardware prototypes have been built to validate the concepts.

2. Directly coupled interleaved boost converter

Fig. 1 shows the schematic diagram of the 3-phase interleaved boost converter with direct coupled inductors.

As the output current is divided by the number of phases, the current stress in each transistor is reduced. Each transistor is switched at the same frequency but at a phase difference of 2Π/3 [7]. Switching sequences of each phase may overlap depending upon the duty ratio (*D*). The duty ratio (*D*) should be greater than 1/3 for the output voltage to be higher than the input voltage. In this case the input voltage to the IBC is 33 V and the desired output voltage is 100 V, therefore *D* has been chosen as 0.67. Fig. 2 shows the switching pattern for the switches for $D = 0.67$.

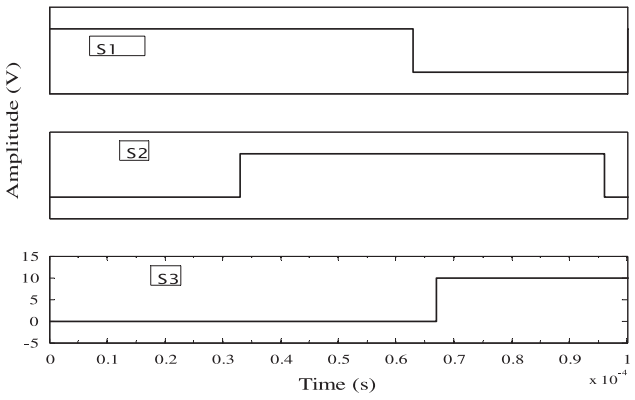

Fig. 2 – Switching Pattern for 3-Phase IBC.

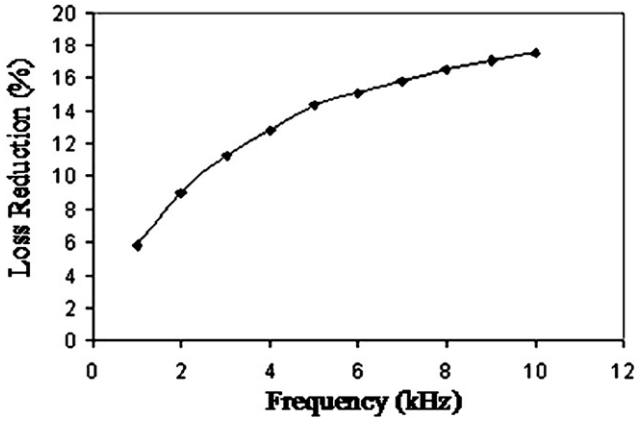

Fig. 3 – Loss reduction in percentage using SiC diode.

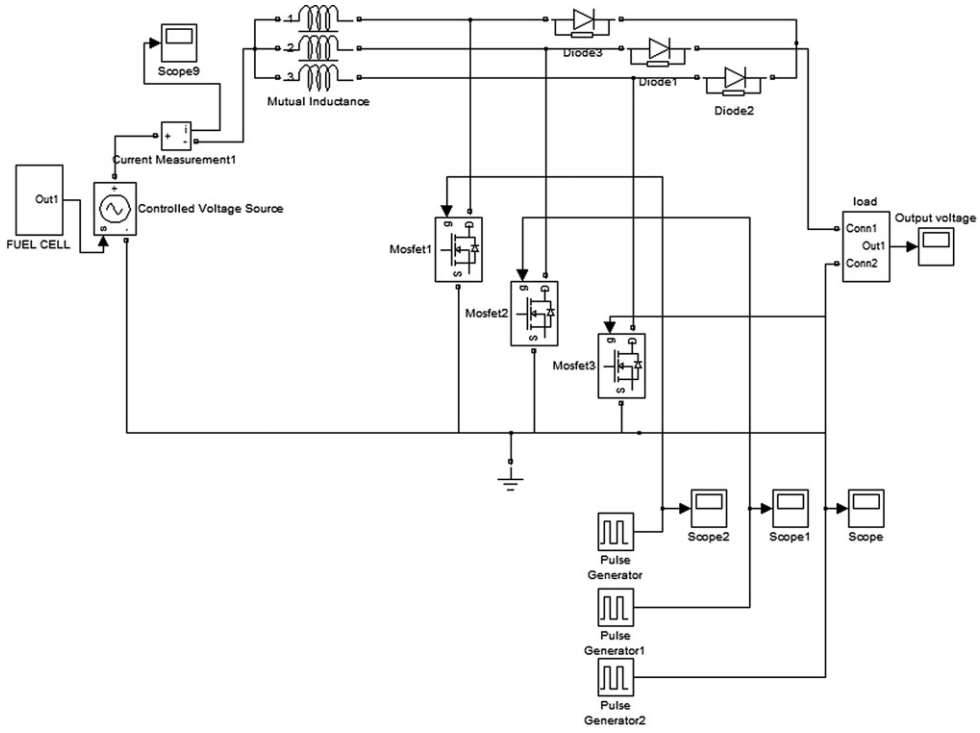

Fig. 4 – SIMULINK diagram for FC interfaced with 3-phase IBC.

3. Design methodology for directly coupled IBC

The steps involved in designing IBC are as follows [8]:

- Selection of Inductor
- Decision of duty ratio and number of phases
- Selection of power semiconductor switches
- Design of output filter

3.1. *Selection of coupled inductor*

The coupled inductor is designed with a ferrite EE core. Each leg of the converter is switched at a frequency of 10 kHz with a phase shift of 120°.

The equivalent inductance expression for directly coupled IBC is

$$L_{eq} = \frac{V_{in}\, DT}{\Delta I_{phase}} \tag{1}$$

The phase current ripple which is decided by L_{eq} is given by

$$\Delta I_{phase} = \frac{V_{in}\, DT}{L} \frac{1 + \alpha + 2\alpha \dfrac{D}{1-D}}{1 + \alpha - 2\alpha^2} \tag{2}$$

To find out the values of L_m and L_k, the input current is calculated using the input voltage and power [8]. With a coupling coefficient (α) of 0.61, the minimum self-inductance of the coupled inductor is found as

$$L = \frac{1 + \alpha \dfrac{D}{1-D}}{1 + \alpha - 2\alpha^2} L_{eq} \tag{3}$$

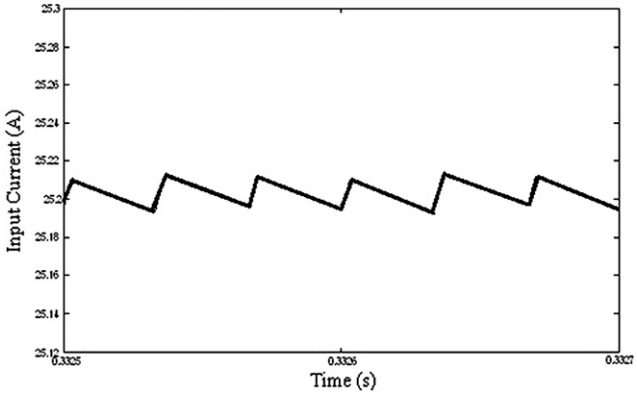

Fig. 5 – Input current waveform for directly coupled IBC.

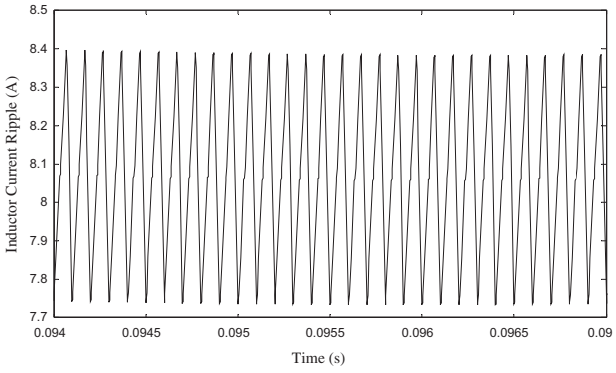

Fig. 6 – Inductor current waveform for directly coupled IBC.

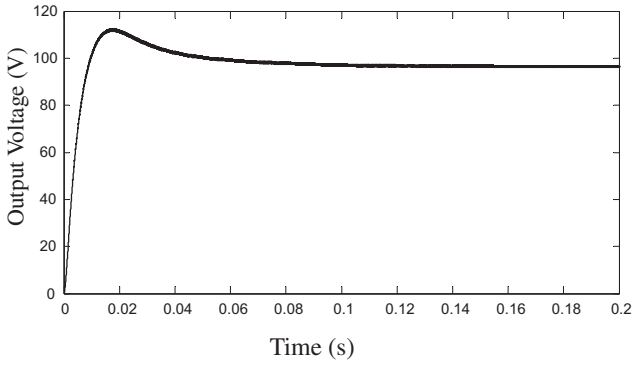

Fig. 7 – Output voltage waveform for 3-phase IBC (V_o = 100 V).

The value of the mutual inductance (L_m) and leakage inductance L_k is calculated as

$$L_m = \alpha \cdot L \tag{4}$$

$$L_k = (1-\alpha)L \tag{5}$$

Therefore, the overall input current ripple is derived as

$$\Delta I_{in} = \frac{V_{in}DT}{L}\left(\frac{(1-\alpha)\left(1-\frac{2D}{1-D}\right)}{1+\alpha-2\alpha^2}\right) \tag{6}$$

From equations (2) and (6), it is clear that increasing the value of the coupling coefficient can effectively reduce the input current ripple, but the phase current ripple is increased [9]. Therefore, the value of coupling coefficient is carefully chosen as 0.61, so that the input current ripple is reduced and the phase current ripples are within the limits [10].

3.2. *Selection of duty ratio and number of phases*

Lower output voltage ripple results in lowering the output capacitance requirements. Therefore, the duty ratio is chosen as 0.67 and the number of phases for IBC as three so as to get reduced input current ripple and keep the inductor current ripple within limits. Compared to uncoupled and inversely coupled inductor, the input current ripple is reduced for directly coupled IBC [10,11].

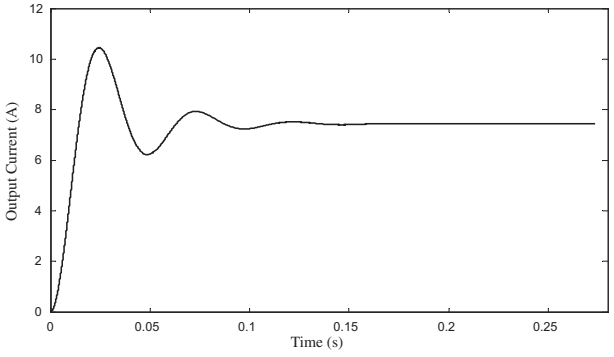

Fig. 8 – Output current waveform for 3-phase IBC (I_o = 7.5 A).

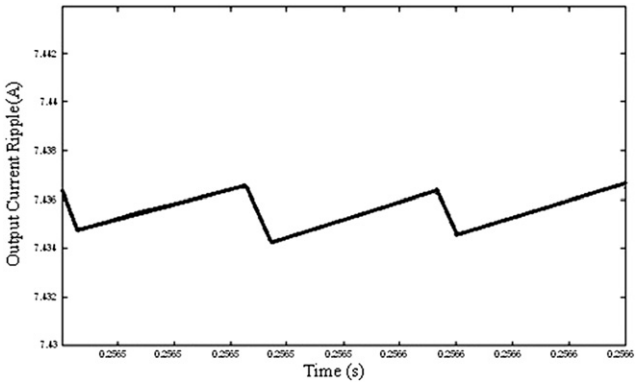

Fig. 9 – Output current ripple (0.026%) waveform for 3-phase IBC.

3.3. *Selection of power devices*

The semiconductor devices chosen for constructing the 3-phase interleaved boost converter is the CoolMOS transistor and SiC diode. The main benefits of CoolMOS are lower on-state résistance, lower conduction losses and high switching operation. The performance of CSD 100060 SiC Schottky diode is compared with that of MUR1560 Si diode for IBC using PSPICE. The SiC diode has less forward voltage, high reverse breakdown voltage and less reverse recovery current which results in reduced switching loss. Due to absence of reverse recovery current, there is no need of active snubber circuit for protection. The loss reduction in percentage using SiC diode is shown in Fig. 3.

Hence, the proper choice of semiconductor switches is important in improving the performance of the converter [11,12].

3.4. *Output filter*

A capacitor filter is needed at the output to limit the peak to peak ripple of the output voltage. The capacitance of the output filter is function of the duty cycle, frequency and minimum load resistance during maximum load [13,14]. For

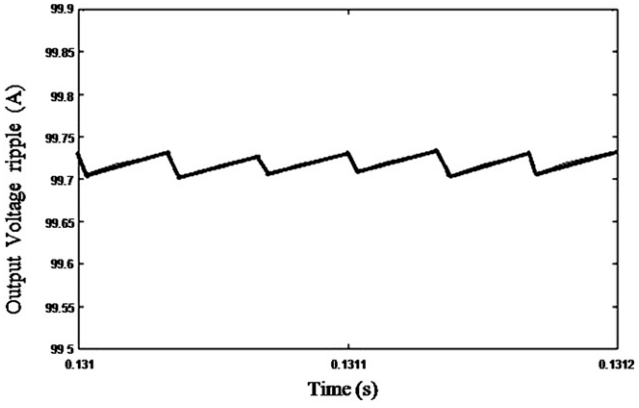

Fig. 10 – Output voltage ripple waveform for 3-phases IBC (0.03%).

Table 1 – Comparison of turn-on, turn-off time and switching energy for CoolMOS and IRFP460A MOSFET (simulation results).

Parameter	IRFP460A MOSFET	CoolMOS Transistor
Turn-on time	120 ns	120 ns
Turn-off time	550 ns	400 ns
Switching energy	500 uJ	310 uJ

Table 2 – Comparison of I_{rr} and t_{rr} for Si and SiC diode.

Parameter	Si Diode	SiC Diode
Reverse recovery current (I_{rr})	100 A	20 A
Reverse recovery time (t_{rr})	60 ns	20 ns

5% output voltage ripple, the value of the capacitance is given by the formula:

$$C = \frac{V_0 DT}{R\Delta V_0} \quad (7)$$

where 'R' represents the load resistance.

4. Simulation results under open-loop control

As per the design equations [15,16], a three-phase interleaved boost converter with directly coupled inductors is simulated in

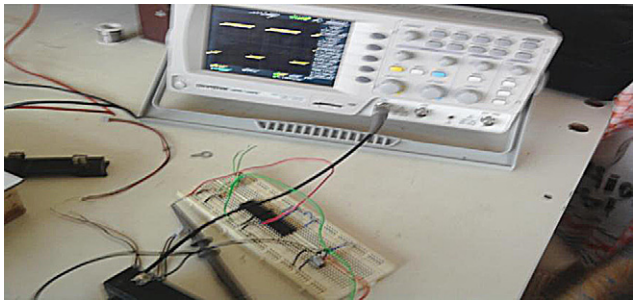

Fig. 11 – PIC microcontroller for pulse generation (switching frequency = 10 kHz).

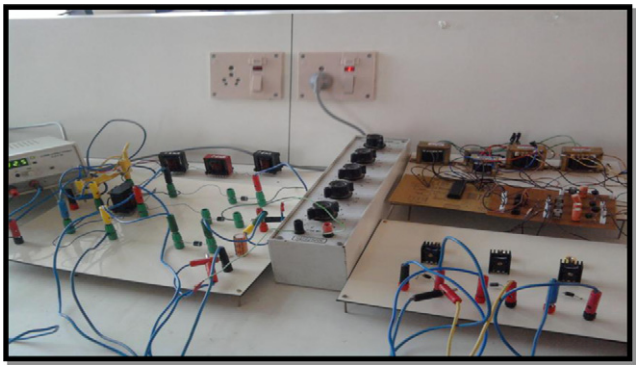

Fig. 12 – A prototype of IBC.

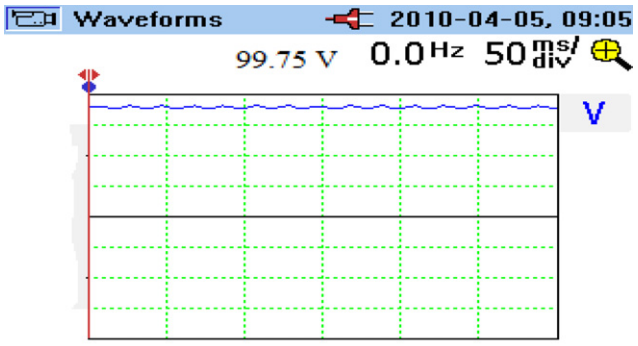

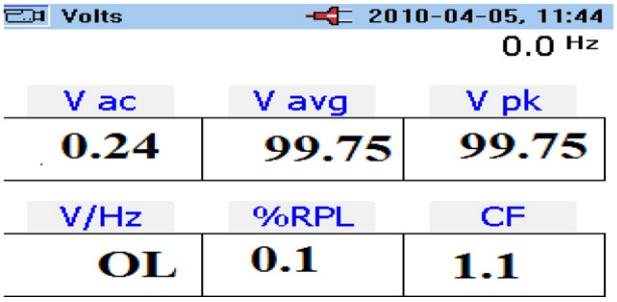

Fig. 13 – Output voltage ripple waveform and ripple factor.

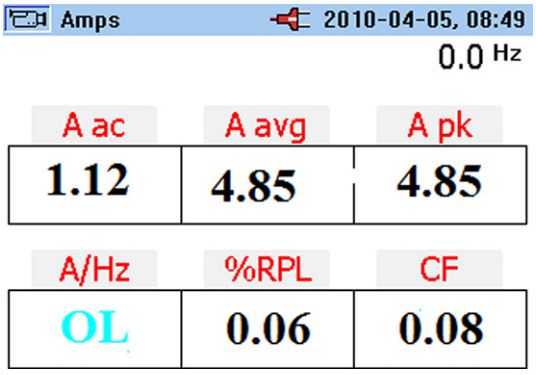

Fig. 14 – Ripple factor for input current ripple.

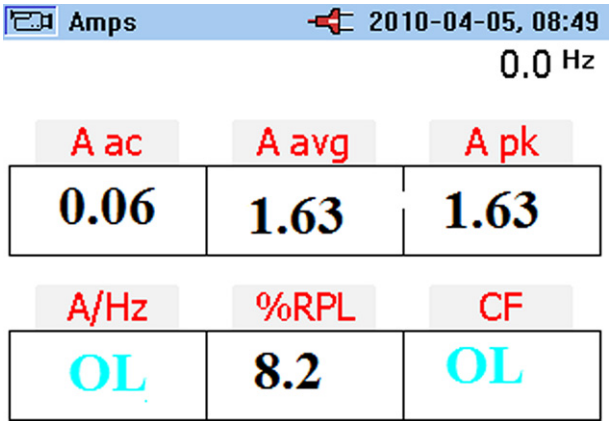

Fig. 15 – Ripple factor for inductor current ripple.

Table 3 – Simulation and experimental results for uncoupled and directly coupled IBC.

Parameters	Uncoupled IBC		Directly Coupled IBC	
	Simulation Results	Experimental Results	Simulation Results	Experimental Results
Input current ripple	0.12%	0.09%	0.04%	0.06%
Inductor current ripple	5.1%	7.95%	7.80%	8.35%
Output voltage ripple	0.03%	0.35%	0.03%	0.1%

MATLAB/SIMULINK using fuel cell as the DC source as shown in Fig. 4. The simulation parameters are summarized as $V_{fc} = 33$ V, $P_0 = 750$ W, $R = 13.33\ \Omega$, $C = 1000$ uF, $f_s = 10$ kHz, $L_m = 4.3$ mH, $L_{k1} = L_{k2} = 7.9$ mH, $V_0 = 100$ V, $D = 0.67$ and $\alpha = 0.61$.

Figs. 5 and 6 show the input current and inductor current ripple waveforms of a directly coupled IBC under steady-state condition.

The inductor current of phase 1 swings between 8.4 A and 7.75 A or 0.65 Ap-p. This average out to 8.075 A with a ripple of 7.80% which is slightly less than the calculated ripple equal to 10%. The input current ripple is about 0.08%. Fig. 7 shows the output voltage waveform for IBC which is settled at 100 V and Fig. 8 shows the output current settled at 7.5 A.

Fig. 9 shows the filtered output current seen during full load. The filtered waveform is once again continuous and possesses both AC and DC component, similar to the input current. The required output current level for this converter is specified to be 7.5 A. The output current ripple is 0.002 A, or 0.026%, well below the required 1% ripple. Fig. 10 shows the output voltage ripple waveform for IBC.

5. Switching loss calculation for IBC

The combination of CoolMOS transistor and SiC diode for the proposed IBC topology results in a reduced switching loss compared to IRFP460A MOSFET and Si diode. Switching loss for the main power device is calculated based on the equation given below [17,18]:

$$P_{sw} = \frac{1}{2} V_0 \frac{I_{in}}{N} (t_{on} + t_r + t_{off} + t_f) f_s \quad (8)$$

where, P_{sw} represents the switching loss of the main power semiconductor device, N represents the number of phases, f_s represents the switching frequency, I_{in} represents the current through the device, V_0 represents the voltage, t_{on} represents the turn-on time of the device, t_{off} represents the turn-off time of the device, t_r represents the current rise time, t_f represents the voltage fall time. The simulated turn-on time, turn-off time and switching energy for CoolMOS transistor and IRFP460A MOSFET is shown in Table 1.

From Table 1, the simulation results shows that CoolMOS transistor has lower switching energy compared to MOSFET.

The diode switching loss is given by

$$P_{swD} = \frac{1}{2} V_0 \frac{I_{RM}}{N} t_{rr} f_s \quad (9)$$

where, P_{swD} represents the diode switching loss, V_0 represents the voltage, N represents the number of phases, t_{rr} represents the reverse recovery time, I_{RM} represents the peak reverse recovery current, f_s represents the switching frequency [19]. The SiC diode chosen for IBC has high reverse breakdown voltage, less reverse recovery current, less reverse recovery time and the simulated results are shown in Table 2.

Table 2 shows that SiC Schottky diode has less reverse recovery time compared to the conventional Si diode.

6. Design and construction of a three-phase IBC

A prototype of a 3-phase directly coupled IBC has been designed in order to verify the simulation results. The hardware set-up consists of the main power circuit, PIC microcontroller board for pulse generation and power supply circuit for optocouplers. The main power circuit consists of three boost converters in parallel with CoolMOS transistors and SiC diodes. The optocoupler 6N137 is used to isolate the power circuit from the PIC circuit. PIC18F4550 is employed to generate the pulses required to trigger the MOSFET with a switching frequency of 10 kHz as shown in Fig. 11.

The overall prototype arrangement is shown in Fig. 12. The output voltage ripple waveform is shown in Fig. 13.

Fig. 14 shows the ripple factor of input current waveform.

Fig. 15 shows the inductor current ripple factor which is below the designed value (10.2%).

Table 3 compares the simulation and experimental results for uncoupled and directly coupled IBC. The results indicate that the directly coupled IBC gives a reduced input current ripple which is best suited for fuel cell applications.

7. Conclusions

This paper has presented the study and design of a three-phase directly coupled IBC for fuel cells. The relationship between phase current ripple, input current ripple versus duty ratio and coupling coefficient is analyzed. The design equations for IBC have been presented. The performance of IBC is studied for uncoupled and directly coupled inductors. It is demonstrated that the directly coupled interleaved DC–DC converter effectively reduces the overall current ripple compared to that of uncoupled inductors. The switching losses of two sets of device combinations for IBC have been compared: the MOSFET IRFP460A and the Si diode MUR1560, the CoolMOS transistor and SiC Schottky diode

CSD 100060. The choice of SiC diode and CoolMOS transistor for IBC has led to reduced switching losses. From these results, directly coupled IBC with CoolMOS transistor and SiC diode proves to be a suitable candidate for fuel cell interface.

REFERENCES

[1] Jain IP. Hydrogen the fuel for 21st century. Int J Hydrogen Energy 1990;15(5):345–8.

[2] Winter CJ. Hydrogen energy-abundant, efficient, clean: a debate over the energy system of change. Int J Hydrogen Energy July 2009;34(14):S1–52.

[3] Peighambardoust SJ, Rowshanzamir S, Amjadi M. Review of the proton exchange membranes for fuel cell applications. Int J Hydrogen Energy Sept.2010;35(17): 9349–84.

[4] Kovacevic G, Tenconi A, Bojoi R. Advanced DC-DC converter for power conditioning hydrogen fuel cell systems. Int J Hydrogen Energy June 2008;33(12):3215–9.

[5] Choe GY, Kang HS, Lee BK, Lee WL. Design consideration of interleaved converters for fuel cell applications. IEEE ICEMS; 2007:238–43. Seoul.

[6] Kosai H, McNeal S, Page A, Jordan B, Scofield J, Ray. B. Characterizing the effects of inductor coupling on the performance of an interleaved boost converter. CARTS USA; 2009:237–51.

[7] Shin HB, Park JG, Chung SK, Lee HW, Lipo TA. Generalized steady-state analysis of multiphase interleaved boost converter with coupled inductors. IEE Electronics Power Appl 2005;152(3):584–94.

[8] Lee P, Lee Y, Cheng DKW, Liu X. Steady-state analysis of an interleaved boost converter with coupled inductors. IEEE Trans Ind Electron 2000;47(4):787–95.

[9] Huber L, Irving BT, Jovanovic. MM. Closed-loop control methods for interleaved DCM/CCM boundary boost PFC converters. IEEE APEC; 2009:991–7.

[10] Thounthong P, Sethakul P, Rael S, Davat B. Design and implementation of 2-phase interleaved boost converter for fuel cell power source. IET ICPEMD; 2008:91–5.

[11] Xu H, Qiao E, Guo X, Wen X, Kong L. Analysis and design of high power interleaved boost converters for fuel cell distributed generation system. IEEE PESC; 2005:140–5.

[12] Veerachary M, Senjyu T, Uezato K. Modeling and analysis of interleaved dual boost converter. IEEE ISIE June 2001;2: 718–22. 2001.

[13] Veerachary M, Senjyu T, Uezato K. Small-signal analysis of interleaved dual boost converter. Int J Circuit Theory Applications 2001;29(6):575–89.

[14] Wai RJ, Duan RY. High step-up converter with coupled-inductor. IEEE Trans Power Electronics 2005;20(5):1025–35.

[15] Dahono PA, Riyadi S, Mudawari A, Haroen. Y. Outputs ripple analysis of multiphase DC-DC converter. IEEE ICPEDS; 1999: 626–31.

[16] Miwa BA, Dtten DM, Schlecht. MF. High efficiency power factor correction using interleaving technique. IEEE APEC 1999;1:557–68.

[17] Todorovic MH, Palma L, Enjeti PN. Design of a wide input range DC-DC converter with a robust power control scheme suitable for fuel cell power conversion. IEEE Trans Ind Electron 2008;55(3):1247–55.

[18] Luo FL, Hong Ye, Rashid. M. Digital power electronics and applications. Academic Press; 2009.

[19] Erickson RW, Maksimovic D. Fundamentals of power electronics. 2nd ed. Kluwer Academic Publishers; 2001.